apparatus. We also very much appreciated helpful discussions with and suggestions from Dr. J. B. Cumming, who called our attention to the method used in correlating the data of this work.

APPENDIX

Since the relationship between energy and reduced velocity, V_r, is one which requires considerable arithmetic, we have prepared Fig. 33 to permit ready conversions between these variables. Three double scales are presented in Fig. 33; in each case the left-hand side is logarithmic, while the right-hand side is linear. To calculate V_r for an ion of kinetic energy E(MeV), atomic number Z, and mass number A, find the MeV/nucleon value under the E/A scale of Fig. 33, and read the value of B. Next find the atomic number on the scale marked Z, and read the corresponding number C.

Finally read the value of V_r on the third log scale opposite the difference $(B-C)$ on the linear scale.

PHYSICAL REVIEW VOLUME 173, NUMBER 2 10 SEPTEMBER 1968

Radiationless Annihilation of Positrons in Lead

SAKAE SHIMIZU, TAKESHI MUKOYAMA, AND YASUYUKI NAKAYAMA
Institute for Chemical Research, Kyoto University, Kyoto, Japan
(Received 23 October 1967; revised manuscript received 20 May 1968)

A process of positron annihilation without emission of radiation, *radiationless* or *zero-quantum annihilation*, has been investigated experimentally. A theory for this phenomenon has also been developed. The 300-keV positrons were focused on a thin lead target by the use of a Siegbahn-Slätis intermediate-image spectrometer mounted with Na^{22} as a positron source. The shell electrons ejected from the lead foil were observed with a lithium-drifted silicon detector mounted immediately behind the foil. We have observed a small peak in the expected energy region of the electron spectrum. This has been attributed to the shell electrons ejected from the lead foil. The effect of target thickness has been examined carefully as an important factor influencing our observations. Using the experimental data obtained, we have attempted to estimate the total cross section of this annihilation process in lead. Our experimental result is $\sigma_{\mathrm{exptl}}=0.8_{-0.8}{}^{+0.4}\times10^{-26}$ cm^2 as a sum of those for K-K, K-L, K-M, and L-L pairs of shell electrons in a lead atom for 300-keV positrons. The calculated cross section we obtained is $\sigma_{\mathrm{calc}}=0.727\times10^{-26}$ cm^2. Our experimental value is in agreement with the calculated result within the experimental error. The present work has established the experimental evidence for this mode of positron annihilation, and has furthered understanding of the process.

1. INTRODUCTION

It is well known that when a positron annihilates in collision with an electron there exist two distinct processes, i.e., annihilation by a free electron and by an electron strongly bound in an atom. In the former case, at least two photons are emitted because of the conservation law of momentum, while in the latter only a single-quantum annihilation can take place. Many theoretical and experimental works on these two types of the annihilation processes have so far been published.

Based on the hole theory of the positron, the single-quantum process can be interpreted as arising from a radiative transition in which an electron bound in an atom falls into a vacant level in the unoccupied continuous negative-energy state. In this case, as a competitive process there may exist a third process by which a positron annihilates without emission of radiation. This mode of annihilation would occur when the single-quantum annihilation takes place with one of the K- or L-shell electrons and when simultaneously the excess energy liberated, instead of being radiated as a photon, is used to eject another shell electron from the atom concerned. The annihilation by this process, therefore, may be called *radiationless annihilation* or *zero-quantum annihilation*. As is shown in Fig. 1, the energy relation between the incident positron, ejected electron, and a pair of the shell electrons involved is very simple. Let E_α and E_β be the total energies (including rest mass) of the two bound electrons concerned in the atom before transition, and let E_+ be that of an incident positron; then the total energy E_- of the electron ejected as a result of the radiationless annihilation is given by

$$E_-=E_++E_\alpha+E_\beta. \tag{1}$$

It is noted that the figure and diagram shown in Fig. 1 are concerned with the process where the total energy of a shell electron with which a positron annihilates is denoted by a subscript α and that of another shell electron before ejection is by a subscript β. Similar figure and diagram are obtained by exchanging α for β in the case where α is for the electron to be ejected and β is for the electron with which a positron annihilates. Equation (1) is valid for both of these cases.

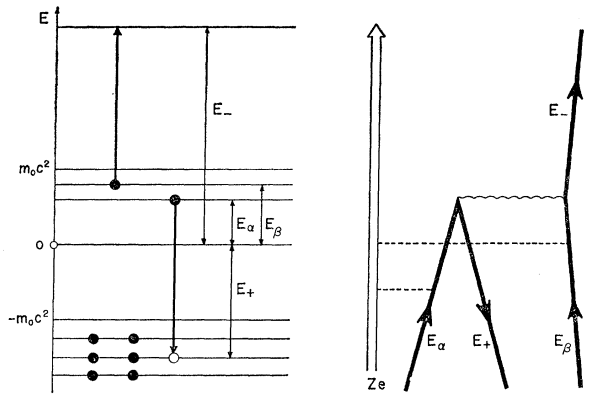

FIG. 1. Diagram for the radiationless annihilation of a positron and the figure illustrating the energy relation between an incident positron and two shell electrons involved in this process.

In 1934 Brunings[1] first pointed out the possibility of this mode of annihilation of the positron and estimated the cross section in the case where the two electrons concerned are both in the K shell of lead. Using nonrelativistic calculations involving a number of approximations, he has shown the cross section for lead to be about 10^{-26} cm^2 for the incident positrons, with kinetic energy being 100–500 keV. More elaborate calculations of the cross section for this process were performed by Massey and Burhop[2] in 1938 by treating various atomic shells rigorously. Their calculations have shown that the total cross section for pairs of electrons in a lead atom would have a maximum value of between 1 and 1.5×10^{-26} cm^2 for incident positrons with kinetic energy of 300 keV.

To our knowledge, excepting our preliminary report[3] in 1965, no experimental study on this phenomenon has so far been published. Owing to such a rather small cross section, to demonstrate this mode of annihilation by experimental evidence an intense monoenergetic positron beam and an energy-selective detector for the ejected electrons are necessary.

In this paper we present essential details of our experimental research on the radiationless annihilation of positrons in a thin lead foil using a monoenergetic positron beam of 300 keV. We have also performed the relativistic calculations of the cross section for this process and compared the results with the experiment, taking into account the repulsive influence of the nucleus, retardation effect, spin-spin interaction, and electron exchange.

II. THEORY

Radiationless annihilation is defined as follows: When an electron bound in an atom undergoes a transition from a positive-energy state to a negative-energy state, giving up energy $k_0=E_--E_\alpha$ or $k_0=E_--E_\beta$, one of the other atomic electrons is lifted from a bound state to a free state, as shown in Fig. 1. The cross section for this process can be written in the retarded form[2]

$$\sigma=\frac{E_+E_-p_-}{(2\pi)^2p_+}\int\delta(E_\alpha+E_\beta+E_+-E_-)\sum|A|^2d\Omega_{p_-}. \quad (2)$$

The matrix element A is given by

$$A=B-C, \quad (3a)$$

where

$$B=e^2\int d\mathbf{r}_1d\mathbf{r}_2\,\phi_+^*(\mathbf{r}_1)\phi_-^*(\mathbf{r}_2)(1-\boldsymbol{\alpha}_1\cdot\boldsymbol{\alpha}_2)\times[\exp(ik_0R)/R]\psi_\alpha(\mathbf{r}_1)\psi_\beta(\mathbf{r}_2), \quad (3b)$$

$$C=e^2\int d\mathbf{r}_1d\mathbf{r}_2\,\phi_+^*(\mathbf{r}_1)\phi_-^*(\mathbf{r}_2)(1-\boldsymbol{\alpha}_1\cdot\boldsymbol{\alpha}_2)\times[\exp(ik_0R)/R]\psi_\beta(\mathbf{r}_1)\psi_\alpha(\mathbf{r}_2). \quad (3c)$$

In these expressions $\sum$ indicates the average over spin directions of the positron and the sums over those of the ejected electron and magnetic quantum numbers of the atomic electrons concerned, $\delta(E_\alpha+E_\beta+E_+-E_-)$ is the usual δ function, $\boldsymbol{\alpha}_1$ and $\boldsymbol{\alpha}_2$ are the Dirac matrices, k_0 is the energy transfer in the transition, e is the charge of an electron, and R is the distance between $\mathbf{r}_1$ and $\mathbf{r}_2$. We denote the energy-momentum vectors of the positron and ejected electron by $(\mathbf{p}_+, iE_+)$ and $(\mathbf{p}_-, iE_-)$, respectively. The wave functions in the matrix element are solutions of the Dirac equation in the Coulomb field of a nucleus: $\psi_\alpha(\mathbf{r})$ and $\psi_\beta(\mathbf{r})$ are for the bound states, $\phi_+(\mathbf{r})$ is for the positron, and $\phi_-(\mathbf{r})$ is for the free electron.

The bound-state Coulomb-field wave function is given by

$$\psi_\mu(\mathbf{r})=\begin{pmatrix} g_\kappa(\lambda r) & \chi_\kappa^\mu(\hat{r}) \\ if_\kappa(\lambda r) & \chi_{-\kappa}^\mu(\hat{r})\end{pmatrix}, \quad (4)$$

where the radial functions f_κ and g_κ are[4]

$$f_\kappa(\lambda r)=-N(1-W)^{1/2}r^{\gamma-1}\exp(-\lambda r)(a_0+a_1r+a_2r^2), \quad (5a)$$

$$g_\kappa(\lambda r)=N(1+W)^{1/2}r^{\gamma-1}\exp(-\lambda r)(c_0+c_1r+c_2r^2). \quad (5b)$$

The angular part of Eq. (4) is expressed by[5]

$$\chi_\kappa^m(\hat{r})=\sum_\tau C(l\tfrac{1}{2}j;\,m-\tau\,\tau)Y_l^{m-\tau}\chi^\tau, \quad (6)$$

where χ^τ are the Pauli spinors, $C(j_1j_2j_3;\,m_1m_2)$ is the

[1] J. Brunings, Physica **1**, 996 (1934).
[2] H. S. W. Massey and E. H. S. Burhop, Proc. Roy. Soc. (London) **A167**, 53 (1938).
[3] S. Shimizu, T. Mukoyama, and Y. Nakayama, Phys. Letters **17**, 295 (1965).
[4] M. E. Rose, *Relativistic Electron Theory* (John Wiley & Sons, Inc., New York, 1961), p. 179.
[5] M. E. Rose, *Elementary Theory of Angular Momentum* (John Wiley & Sons, Inc., New York, 1957), p. 152.

Clebsch-Gordan coefficient, $Y_l^m(\hat{r})$ are the spherical harmonics, $\kappa=\mp(j+\frac{1}{2})$ for $j=l\pm\frac{1}{2}$, and $\hat{r}$ is a unit vector in the direction of $\mathbf{r}$.

The continuum-state solution of the Dirac equation for a Coulomb field is[6]

$$\phi_-(\mathbf{r})=4\pi\sum_{\kappa m}P_{\kappa m}(\hat{p},\hat{\xi})i^l\exp(-i\delta_\kappa')\times\begin{pmatrix}g_\kappa(r) & \chi_\kappa^m(\hat{r})\\ if_\kappa(r) & \chi_{-\kappa}^m(\hat{r})\end{pmatrix},\quad(7)$$

where $\hat{\xi}$ is a unit vector in the direction of the electron's spin, the κ sum runs over all nonzero integers, and

$$P_{\kappa m}(\hat{p},\hat{\xi})=\chi_\kappa^{m*}(\hat{p})\chi^\xi,$$

$$\delta_\kappa'=\eta-\tfrac{1}{2}\pi\gamma-\arg\Gamma(\gamma+iy)+\tfrac{1}{2}(l+1)\pi.$$

The radial functions are

$$rf_\kappa(r)=i\left(\frac{W-1}{2W}\right)^{1/2}\frac{(2pr)^\gamma\exp[\frac{1}{2}(\pi y)]\,|\,\Gamma(\gamma+iy)\,|}{2p\Gamma(2\gamma+1)}\times\{\exp(-ipr+i\eta)(\gamma+iy)\times F(\gamma+1+iy,\,2\gamma+1,\,2ipr)-\text{c.c.}\},\quad(8a)$$

$$rg_\kappa(r)=\left(\frac{W+1}{2W}\right)^{1/2}\frac{(2pr)^\gamma\exp[\frac{1}{2}(\pi y)]\,|\,\Gamma(\gamma+iy)\,|}{2p\Gamma(2\gamma+1)}\times\{\exp(-ipr+i\eta)(\gamma+iy)\times F(\gamma+1+iy,\,2\gamma+1,\,2ipr)+\text{c.c.}\},\quad(8b)$$

with

$$\gamma=(\,|\,\kappa\,|^2-\alpha^2Z^2)^{1/2},\qquad y=\alpha ZW/p,\qquad \alpha=e^2,$$

and

$$\exp(2i\eta)=-(\kappa-iy/W)/(\gamma+iy).$$

The positron wave function, which is chosen to represent asymptotically a distorted plane wave with an ingoing spherical wave, is

$$\phi_+(\mathbf{r})=4\pi\sum_{\kappa m}P_{\kappa m}(\hat{p},-\hat{\xi})i^l\exp(-i\delta_\kappa')\times\begin{pmatrix}-if_\kappa^c(r) & \chi_{-\kappa}^m(\hat{r})\\ g_\kappa^c(r) & \chi_\kappa^m(\hat{r})\end{pmatrix},\quad(9)$$

in which f_κ^c and g_κ^c are the same forms with the radial functions for the electron but with the sign of Z reversed. The normalization of these continuum radial functions is done by matching them with the asymptotic forms at large distance:

$$f_\kappa(r)\underset{r\to\infty}{\longrightarrow}[(W-1)/2W]^{1/2}(pr)^{-1}\sin(pr+\delta_\kappa),\quad(10a)$$

$$g_\kappa(r)\underset{r\to\infty}{\longrightarrow}[(W+1)/2W]^{1/2}(pr)^{-1}\cos(pr+\delta_\kappa),\quad(10b)$$

where

$$\delta_\kappa=y\ln(2pr)-\arg\Gamma(\gamma+iy)+\eta-\tfrac{1}{2}\pi\gamma.$$

We now introduce the well-known expression for the retardation factor:

$$\frac{\exp(ik_0R)}{4\pi R}=ik_0\sum_{lm}h_l(k_0r_>)j_l(k_0r_<)Y_l^{m*}(\hat{r}_1)Y_l^m(\hat{r}_2),\quad(11)$$

where j_l is the spherical Bessel function of order l, h_l is the spherical Hankel function of the first kind, and $r_>$ is the greater and $r_<$ the lesser of r_1 and r_2. Using the above representations, Eqs. (4), (7), and (9) for the electron and positron wave functions, and inserting Eq. (11) into Eq. (3b), the matrix element becomes

$$B=-(4\pi)^3e^2k_0\sum_{\kappa_1m_1}\sum_{\kappa_2m_2}\sum_{lm}i^{-(l_1+l_2)}\times\exp[i(\delta_{\kappa_1}'+\delta_{\kappa_2}')]P_{\kappa_1m_1}^*(\hat{p}_+,-\hat{\xi}_1)P_{\kappa_2m_2}^*(\hat{p}_-,\hat{\xi}_2)\times\{B_{-\kappa_1\kappa_2\kappa_3\kappa_4}I_{\kappa_1\kappa_2l}^{(1)}+B_{-\kappa_1-\kappa_2\kappa_3-\kappa_4}I_{\kappa_1\kappa_2l}^{(2)}+B_{\kappa_1\kappa_2-\kappa_3\kappa_4}I_{\kappa_1\kappa_2l}^{(3)}+B_{\kappa_1-\kappa_2-\kappa_3-\kappa_4}I_{\kappa_1\kappa_2l}^{(4)}+B'_{-\kappa_1\kappa_2-\kappa_3-\kappa_4}I_{\kappa_1\kappa_2l}^{(5)}-B'_{-\kappa_1-\kappa_2-\kappa_3\kappa_4}I_{\kappa_1\kappa_2l}^{(6)}-B'_{\kappa_1\kappa_2\kappa_3-\kappa_4}I_{\kappa_1\kappa_2l}^{(7)}+B'_{\kappa_1-\kappa_2\kappa_3\kappa_4}I_{\kappa_1\kappa_2l}^{(8)}\},\quad(12)$$

where the subscript 1 refers to the incident positron, 2 to the ejected electron, 3 and 4 to the atomic electrons concerned. The radial integrals $I_{\kappa_1\kappa_2l}^{(1)}\cdots I_{\kappa_1\kappa_2l}^{(8)}$

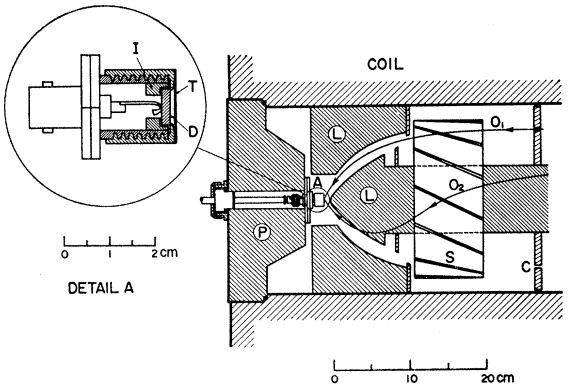

FIG. 2. Experimental arrangement of a thin lead target and lithium-drifted silicon junction detector in the β-ray spectrometer. Positron trajectories are shown by O_1 (distance from the axis) and O_2 (vertical projection). (T) lead target, (D) silicon detector, (I) insulator, (P) polepiece, (L) lead shield, (S) spiral baffle, and (C) annular slit.

[6] M. E. Rose, Phys. Rev. 51, 484 (1937).

appearing in Eq. (12) are given by

$$I_{\kappa_1\kappa_2 l}^{(1)}=\iint f_{\kappa_1}{}^{c*}(r_1)\,g_{\kappa_3}(\lambda r_1)\,g_{\kappa_2}{}^{*}(r_2)\,g_{\kappa_4}(\lambda r_2)\,h_l(k_0 r_>)\,j_l(k_0 r_<)\,r_1^2 r_2^2 dr_1 dr_2, \tag{13a}$$

$$I_{\kappa_1\kappa_2 l}^{(2)}=\iint f_{\kappa_1}{}^{c*}(r_1)\,g_{\kappa_3}(\lambda r_1)\,f_{\kappa_2}{}^{*}(r_2)\,f_{\kappa_4}(\lambda r_2)\,h_l(k_0 r_>)\,j_l(k_0 r_<)\,r_1^2 r_2^2 dr_1 dr_2, \tag{13b}$$

$$I_{\kappa_1\kappa_2 l}^{(3)}=\iint g_{\kappa_1}{}^{c*}(r_1)\,f_{\kappa_3}(\lambda r_1)\,g_{\kappa_2}{}^{*}(r_2)\,g_{\kappa_4}(\lambda r_2)\,h_l(k_0 r_>)\,j_l(k_0 r_<)\,r_1^2 r_2^2 dr_1 dr_2, \tag{13c}$$

$$I_{\kappa_1\kappa_2 l}^{(4)}=\iint g_{\kappa_1}{}^{c*}(r_1)\,f_{\kappa_3}(\lambda r_1)\,f_{\kappa_2}{}^{*}(r_2)\,f_{\kappa_4}(\lambda r_2)\,h_l(k_0 r_>)\,j_l(k_0 r_<)\,r_1^2 r_2^2 dr_1 dr_2, \tag{13d}$$

$$I_{\kappa_1\kappa_2 l}^{(5)}=\iint f_{\kappa_1}{}^{c*}(r_1)\,f_{\kappa_3}(\lambda r_1)\,g_{\kappa_2}{}^{*}(r_2)\,f_{\kappa_4}(\lambda r_2)\,h_l(k_0 r_>)\,j_l(k_0 r_<)\,r_1^2 r_2^2 dr_1 dr_2, \tag{13e}$$

$$I_{\kappa_1\kappa_2 l}^{(6)}=\iint f_{\kappa_1}{}^{c*}(r_1)\,f_{\kappa_3}(\lambda r_1)\,f_{\kappa_2}{}^{*}(r_2)\,g_{\kappa_4}(\lambda r_2)\,h_l(k_0 r_>)\,j_l(k_0 r_<)\,r_1^2 r_2^2 dr_1 dr_2, \tag{13f}$$

$$I_{\kappa_1\kappa_2 l}^{(7)}=\iint g_{\kappa_1}{}^{c*}(r_1)\,g_{\kappa_3}(\lambda r_1)\,g_{\kappa_2}{}^{*}(r_2)\,f_{\kappa_4}(\lambda r_2)\,h_l(k_0 r_>)\,j_l(k_0 r_<)\,r_1^2 r_2^2 dr_1 dr_2, \tag{13g}$$

$$I_{\kappa_1\kappa_2 l}^{(8)}=\iint g_{\kappa_1}{}^{c*}(r_1)\,g_{\kappa_3}(\lambda r_1)\,f_{\kappa_2}{}^{*}(r_2)\,g_{\kappa_4}(\lambda r_2)\,h_l(k_0 r_>)\,j_l(k_0 r_<)\,r_1^2 r_2^2 dr_1 dr_2, \tag{13h}$$

and the angular coupling coefficients by

$$B_{\kappa_1\kappa_2\kappa_3\kappa_4}=(-1)^{m_1+m_2+m+1}(4\pi[l])^{-1}([j_1][j_2][j_3][j_4][l_1][l_2][l_3][l_4])^{1/2}$$
$$\times C(l_1 l_3 l;\,oo)\,C(l_2 l_4 l;\,oo)\,C(j_1 j_3 l;\,-m_1 m_3)\,C(j_2 j_4 l;\,-m_2 m_4)\times W(j_1 j_3 l_1 l_3;\,l_2^{\frac{1}{2}})\,W(j_2 j_4 l_2 l_4;\,l_2^{\frac{1}{2}})\,\delta_{m_3-m_1,m}\,\delta_{m_4+m,m_2}, \tag{14a}$$

$$B'_{\kappa_1\kappa_2\kappa_3\kappa_4}=(-1)^{m_3-m_1}(6[l]/4\pi)\,([j_3][j_4][l_3][l_4])^{1/2}\,C(l_3 l l_1;\,oo)\,C(l_4 l l_2;\,oo)$$
$$\times\sum_{f_1 f_2}([f_1][f_2])^{1/2}\,W(l l_3 j_1 l_2^{\frac{1}{2}};\,l_1 f_1)\,W(l l_4 j_2 l_2^{\frac{1}{2}};\,l_2 f_2)\,W(1\tfrac{1}{2} f_1 l_3;\,\tfrac{1}{2} j_3)$$
$$\times W(1\tfrac{1}{2} f_2 l_4;\,\tfrac{1}{2} j_4)\,C(j_3 1 f_1;\,m_3 m_1+m-m_3)\,C(j_4 1 f_2;\,m_4 m_2-m-m_4)$$
$$\times C(l f_1 j_1;\,-m m_1+m)\,C(l f_2 j_2;\,m m_2-m)\,\delta_{m_1+m_2,m_3+m_4}, \tag{14b}$$

where $[j]=2j+1$ and $W(abcd;\,ef)$ is the Racah coefficient. The matrix element C can be easily obtained from Eq. (12) by exchanging (j_3, l_3, m_3) for (j_4, l_4, m_4). With the aid of these representations, we can obtain the matrix element A.

Squaring the matrix element A, summing over ζ_1 and ζ_2, and integrating over the solid angle Ω_{p_-}, we can then carry out the sums over m, m_1, m_2, m_3, and m_4. The resulting expression is given in the form of products of the radial integrals [Eqs. (13a)–(13h)] and angular coupling coefficients expressed by Clebsch-Gordan coefficients, Racah coefficients, and 9-j symbols. The analytical expression of the total cross section for the radiationless annihilation thus obtained from Eq. (2) is given in the Appendix. The calculated numerical values are discussed in Sec. V.

III. EXPERIMENTAL PROCEDURE

A monoenergetic positron beam was obtained by the use of a Siegbahn-Slätis intermediate-image spectrometer mounted with Na^{22} as a positron emitter. The source was prepared from radioactive sodium chloride solution of high specific activity obtained from the Radiochemical Centre at Amersham. An evaporation residuum of this solution was mounted on a slightly concave hole of 2.5 mm diam on a surface of pure aluminum foil. Total intensity of Na^{22} in this source was estimated to be about 12 mCi, but the effective intensity of this source as a positron emitter was much smaller than this value, owing to the rather large amount (about 2.0 mg) of solids in the evaporation residuum. In the present work the kinetic energy of

the positrons, selected by using the spectrometer, was fixed at 300 keV, near the maximum of the positron spectrum of Na^{22}, to secure the highest possible beam intensity. Our instrument has a spiral separation baffle by which a very high electron-to-positron rejection ratio of about 2×10^{-5} can be achieved. By adjusting properly the widths of an annular slit situated at the midpoint of the instrument and of the other slit set in front of the Na^{22} source, the momentum resolution and over-all transmission of the spectrometer were made to be about 1.8 and 4.0%, respectively, for the 300-keV positrons. The focus of the positron beam on the thin lead target was found to be about 6 mm diam. The positrons hit the target at an angle of incidence of about 60°.

A thin lead foil of 75.3 mg/cm² was placed at the focus point of the spectrometer as the target. This thickness was chosen so as to be the product of sec60° times the thickness of the foil nearly equal to the range of a 300-keV positron in lead, taking account of its angle of incidence on the lead target. As shown in Fig. 2, a lithium-drifted silicon junction detector was mounted 1.0 mm behind the lead target as an energy-selective detector for the shell electrons ejected from the target by the annihilation process to be studied. This *p-i-n* junction detector of 8 mm diam, with an *i*-layer of 2 mm thickness, was prepared by the authors.[7] The pulses from the detector were observed with a 400-channel pulse-height analyzer. The spectra of the resulting pulses from the detector mounted at the focus point of the spectrometer, and then the spectra from the same detector covered with a lead foil whose thickness was equal to that of the lead target used in the present work, were observed for various definite kinetic energies of the incident electrons. By this procedure the energy resolution and peak-to-total ratio for the incident monoenergetic electrons were revealed as 4.3% and 0.60, respectively, for the presumed kinetic energy of the ejected electrons from the lead target by the radiationless annihilation for the *K-K* pair.

The number of 300-keV positrons impinging upon a lead target could be measured by this silicon detector mounted at the focus point, because the effective intensity of the Na^{22} source was much weaker than we expected, owing to the self-absorption in the residuum contained in this source. The detection efficiency of the detector for positrons of this energy, ϵ_p, was estimated by comparing the counts with those measured by a Geiger-Müller (GM) counter with an 8-mm-diam window made of 0.625-mg/cm²-thick rubber hydrochloride mounted at the focus point. In this case, taking into consideration the resolving time of the GM counter, another Na^{22} source of lower intensity was used. By a similar procedure but using a P^{32} source we could estimate also ϵ_e, i.e., the detection efficiency for electrons with energies which would be expected for the shell electrons ejected from the lead target produced by the process to be studied. Here, the detection efficiencies of the GM counter with such a thin window for these positrons and electrons were supposed to be 100%. A ratio ϵ_p/ϵ_e was thus estimated reasonably to be 1.00 ± 0.05.

Long-time operation of the apparatus was required for observation of the electron spectrum of the ejected shell electrons and therefore good stability of the whole measuring system was essential. Stability of gains of the detector and electronic system was checked before and after each 12-h experimental run. The data were printed out every 12 h and only the runs without noticeable drift were summed as the final result.

IV. EVALUATION OF EFFECT OF TARGET THICKNESS

In the observed spectrum of the ejected electrons from the lead target a peak due to the radiationless annihilation process can be expected. However, this peak would be smeared out owing to the effect of the target thickness (75.3 mg/cm²), including degradation of kinetic energies of incident positrons and ejected electrons in the lead foil. For estimation of the number of ejected electrons from the observed curve, consideration of its reasonable profile is necessary, taking account of the effect of the target thickness, energy resolution of the solid detector, and the geometrical arrangement of the target and detector. Since the rigorous treatment of the problem is very difficult, an approximate solution has been developed using theoretical and experimental procedures based upon some appropriate assumptions.

Assumptions adopted to simplify the problem are as follows: (1) The 300-keV positrons impinge upon the central focus area (6 mm diam) of the lead foil at an angle of incidence equal to 60°. (2) The target foil is so thin that any appreciable angular deflection can be neglected for the incident positrons in the target before the annihilation and for the ejected electrons before escaping from the target. (3) The angular distribution of the ejected electrons from any pair of shell electrons by this annihilation process is supposed to be approximately the same form as that expected for those from the *K-K* pair. This angular distribution can be evaluated by combining theoretically that of photons from the single-quantum annihilation and that of photoelectrons from the *K* shell of the atom concerned by the photoelectric effect of the above photons.

The geometry for detecting the ejected shell electrons and the mathematical terms used in the present calculations are shown schematically in Fig. 3. The incident positrons with kinetic energy of $E_0=300$ keV enter into the target foil at an angle of incidence of

[7] S. Nishiu, T. Nakakado, Y. Nakayama, and S. Shimizu, Bull. Inst. Chem. Res., Kyoto Univ. **42**, 319 (1964).

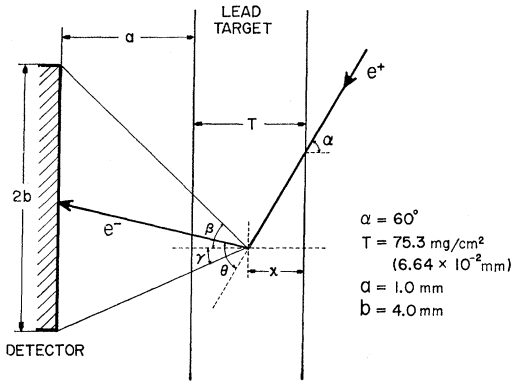

FIG. 3. Schematic diagram illustrating terms used for evaluation of the effect of the target thickness.

$\alpha=60°$. As these positrons penetrate into the foil their energy and number decrease because of various interactions with the target atoms, such as annihilation in flight and scattering. The number of positrons at a distance x from the surface of the target can be expressed by a function $N(E, x)$, where E is the kinetic energy of the positrons at x. Let the total cross section per atom for the radiationless annihilation of positrons with kinetic energy E be $\sigma(E)$; then the rate of this process for the positron energy between E and $E+dE$ in a slab of width dx at x is given by

$$G(E, x)dEdx=N(E, x)n\sigma(E)dEdx, \qquad (15)$$

where n is the number of atoms per unit volume of the target. The kinetic energy of the shell electron ejected by this process can be given according to Eq. (1) by $E'=E+2m_0c^2-B_\alpha-B_\beta$, where m_0 is the rest mass of electron and B_α and B_β are binding energies of the shell electrons involved. The ejected electron traverses a distance $(T-x)/\cos(\theta-\alpha)$ before escaping from the foil, as shown in Fig. 3, where T is a thickness of the target ($T=6.64\times10^{-2}$ mm) and θ is the angle between the direction of momentum of the incident positron and that of the ejected electron. By $K(E, E'; x, \theta)$ we denote the probability that this ejected electron with initial energy E' escapes from the target and is detected by the detector with energy between E'' and $E''+dE''$. The number of electrons which escape from the target and are detected by the detector of diameter $2b$ (8.0 mm), placed at a distance $a=1.0$ mm from the target, can be expressed as

$$R(E'')dE''=\sum_{\text{all electron pairs}}\int_0^T\int_0^{E_0}\int_{\alpha-\gamma}^{\alpha+\beta}K(E, E''; x, \theta)\times G(E, x)P(\theta)\sin\theta\, d\theta dEdxdE'', \qquad (16)$$

where the summation is over all the pairs of shell electrons involved and $P(\theta)$ is the angular distribution of the ejected electrons. From Fig. 3, β and γ are given, respectively, by

$$\tan\beta=(b+x\tan\alpha)/(a+T-x), \qquad (17a)$$

$$\tan\gamma=(b-x\tan\alpha)/(a+T-x). \qquad (17b)$$

Since in the present case both T and x are very small compared with a and b, we can write

$$\tan\beta\approx\tan\gamma\approx b/a\equiv\tan\delta. \qquad (18)$$

Using this relation and Eq. (15), Eq. (16) becomes

$$R(E'')dE''=n\sum_{\text{all electron pairs}}\int_0^T\int_0^{E_0}\int_{\alpha-\delta}^{\alpha+\delta}N(E, x)\sigma(E)\times K(E, E''; x, \theta)P(\theta)\sin\theta\, d\theta dEdxdE''. \qquad (19)$$

$R(E'')dE''$ given by this expression represents the energy distribution of the ejected shell electrons detected by the solid detector.

The positron spectrum $N(E, x)$ in Eq. (19) can be obtained by solving a space-dependent transport equation for positrons. It is, however, very difficult to solve such an equation even numerically because of mathematical complexities which arise from the boundary conditions imposed by the experimental configuration and from a variety of interactions that must be taken into account. These include elastic and inelastic scatterings, annihilation, and energy loss by radiation. For this reason, we have attempted to find $N(E, x)$ experimentally by observing the energy spectrum of positrons passed through targets of various thicknesses.

Using lead foils of thicknesses being 13.1, 26.7, 35.0, 51.6, 65.7, and 75.3 mg/cm², energy spectra of positrons passed through these foils were measured for positrons of incident energy of 300 keV by attaching them immediately before the silicon detector mounted at the focus of the β-ray spectrometer. Each positron spectrum thus obtained was considered to give an approximation to the energy spectrum of positrons inside the lead target used at the corresponding thickness, neglecting the difference in the boundary condition. By this procedure we could evaluate $N(E, x)$.

To estimate the electron detection probability $K(E, E''; x, \theta)$ similar measurements with incident electrons with different energies were performed by replacing the Na^{22} source by a P^{32} source and using the lead foils of thicknesses mentioned above. The minimum energy of ejected electrons from this annihilation process is easily obtained from Eq. (1) as 846 keV, corresponding to the case where the positron of zero kinetic energy annihilates with the K-K pair, while the maximum energy is 1290 keV, which corresponds to the 300-keV positron and the L-L pair. Taking account of these values, 11 incident energies of electrons were then chosen as E'; 846, 896, 946, 996, 1046, 1096, 1146, 1180, 1218, 1250, and 1290 keV. From experimental data thus obtained, the electron detection probability for $\theta=0$, $K(E, E''; T-x, 0)$

could be evaluated as a ratio of the number of electrons detected in the channel corresponding to the kinetic energy of E'' to the total number of incident electrons with kinetic energy E'. Since $K(E, E''; x, \theta)$ is a function of $(T-x)/\cos(\theta-\alpha)$, $K(E, E''; x, \theta)$ could be easily evaluated from the experimental values of $K(E, E''; T-x, 0)$ using the Lagrange interpolation and extrapolation formula for x and θ.

The angular distribution of the ejected shell electrons, $P(\theta)$ in Eq. (19), was evaluated, on the basis of the assumption (3) mentioned above, by considering first the angular distribution of photons from the single-quantum annihilation calculated by Johnson[8] and then that of electrons from the photoelectric effect obtained by Pratt *et al.*[9] When we note the direction of a photon emission from the single-quantum annihilation with respect to that of an incident positron is (θ_s, φ_s) and the direction of a photoelectron with respect to that of the above photon is (θ_p, φ_p), then the direction of a photoelectron with respect to that of an incident positron (θ, φ) can be given by the following relations:

$$\cos\theta=\cos\theta_s\cos\theta_p+\sin\theta_s\sin\theta_p\cos\varphi_p,$$
$$\cos(\varphi-\varphi_s)=(\cos\theta_p-\cos\theta_s\cos\theta)/(\sin\theta_s\sin\theta). \quad (20)$$

Using the differential cross section for the single-quantum annihilation, $d\sigma_s/d\Omega_s$, and that for the photoelectric effect, $d\sigma_p/d\Omega_p$, satisfying the trigonometric relationships (20), the probability that the bound electron be emitted into a unit solid angle in the direction (θ, φ) can be expressed as

$$P(\theta, \varphi)=\frac{d\sigma_s}{d\Omega_s}\frac{d\sigma_p}{d\Omega_p}\Big/\int\frac{d\sigma_s}{d\Omega_s}\frac{d\sigma_p}{d\Omega_p}d\Omega. \quad (21)$$

This calculation is very difficult, because $d\sigma_s/d\Omega_s$ and $d\sigma_p/d\Omega_p$ cannot be expressed simply as analytical forms. Instead of the use of Eq. (21), known numerical values of these differential cross sections[8,9] for discrete values of θ_s and θ_p were used as distribution functions, and then values of θ_s and θ_p were determined by generating uniform pseudorandom numbers r_1 and r_2. The selection of a random azimuthal angle φ_p from a uniform distribution on the interval $[0, 2\pi]$ was performed using two random numbers r_3 and r_4 satisfying the condition $r_3^2+r_4^2\leq 1$, and a relation

$$\cos\varphi_p=(r_3^2-r_4^2)/(r_3^2+r_4^2).$$

Using the numerical values of θ_s, θ_p, and φ_p obtained by this procedure the value of $\cos\theta$ given by Eq. (20) could be calculated. Since the detection geometry of the present experiment is axially symmetric, $P(\theta, \varphi)$ is independent of φ. By applying the sampling technique to this $\cos\theta$ the distribution function $P(\theta)$ was obtained. It is noted, however, that such a procedure to calculate the angular distribution of the ejected electrons from the radiationless annihilation is only approximate, because this mode of annihilation is a direct process involving an incident positron and two shell electrons, one of which is ejected with the excess energy liberated.

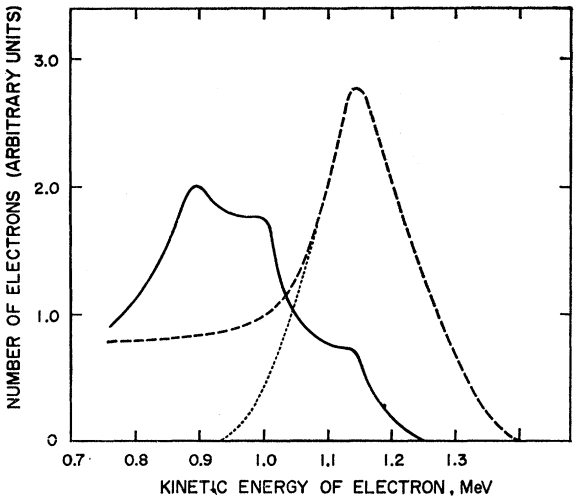

FIG. 4. The expected spectrum of the ejected shell electrons, which should be observed with the present experimental system. The solid curve shows that obtained by taking account of the effect of the target thickness. The dashed curve shows that obtained when this effect is not taken into account. The dotted curve is the presumed slope of the dashed peak representing the total absorption peak of the ejected shell electrons when such an effect can be neglected.

As the total cross section $\sigma(E)$ in Eq. (19), for the K-K pair we used the values calculated by the method mentioned in Sec. II (see Fig. 7). For other pairs of shell electrons it was assumed that energy dependence of the cross section is the same form as that for the K-K pair. The normalization for the total cross section for any of the other pairs was made at the positron kinetic energy of 300 keV using the theoretical values for $\sigma_{\text{other}}(300\text{ keV})$ and $\sigma_{K-K}(300\text{ keV})$ calculated in Sec. II (see Table I). Then $\sigma_{\text{other}}(E)$ for arbitrary energy E is written as

$$\sigma_{\text{other}}(E)=\frac{\sigma_{\text{other}}(300\text{ keV})}{\sigma_{K-K}(300\text{ keV})}\sigma_{K-K}(E). \quad (22)$$

By the use of these experimental data of $N(E, x)$ and $K(E, E''; x, \theta)$, and of the calculated values of $P(\theta)$ and $\sigma(E)$, Eq. (19) for $R(E'')$ could be integrated numerically using our electronic computer.[10] By these complicated procedures the spectrum of the ejected shell electrons detected was obtained, as shown by the solid curve in Fig. 4. It is conceivable that this spectrum may give the reasonable profile expected from our observation of the spectrum, which is due to the annihilation process with 300-keV incident positrons.

[8] W. R. Johnson, Phys. Rev. **159**, 61 (1967).
[9] R. H. Pratt, R. D. Levee, R. L. Pexton, and W. Aron, Phys. Rev. **134**, A898 (1964).
[10] Kyoto University Digital Computer KDC-II; commercial name is HITAC-5020.

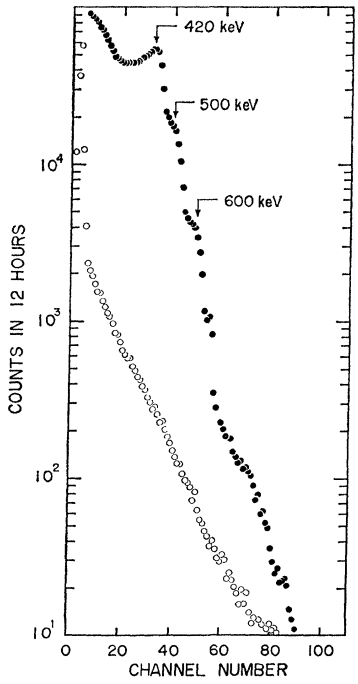

FIG. 5. Solid circles show the electron spectrum in the low-energy region observed by the silicon detector. Open circles show the background contributions from the strayed γ rays and natural background.

If the effect of the target thickness is assumed to be negligible, we get the following equation:

$$G_0(x)\,dx = nN_0\sigma(E_0)\,\sec\alpha\,dx, \tag{23}$$

where N_0 is the total number of positrons incident on the target. This equation corresponds to Eq. (15) in the case where the effect of the target thickness is taken into account. The number of ejected shell electrons entering the detector with kinetic energy between E'' and $E''+dE''$ can be expressed by

$$\begin{aligned} R_0(E'')\,dE'' &= \sum_{\text{all electron pairs}} \int_0^T \int_{\alpha-\gamma}^{\alpha+\beta} G_0(x) \\ &\times K(E_0, E''; T, \theta) P(\theta)\,\sin\theta\,d\theta dx dE'' \\ &= nN_0 T\,\sec\alpha \sum_{\text{all electron pairs}} \sigma(E_0) \\ &\times \int_{\alpha-\delta}^{\alpha+\delta} K(E_0, E''; T, \theta) P(\theta)\,\sin\theta\,d\theta dE''. \end{aligned} \tag{24}$$

This expression gives the energy spectrum of the ejected electrons when the effect of the target thickness is neglected. The spectrum obtained by integrating Eq. (24) numerically is shown by the dashed curve in Fig. 4.

The discussion and results mentioned in this section were taken into consideration when we estimated the total cross section of the process, as described in the following section.

V. RESULTS AND DISCUSSION

The observed spectrum obtained is shown by solid circles in Fig. 5. The relation of channel number versus energy of electrons incident upon the lead target before the silicon detector was calibrated using a P^{32} source. An evident peak at about 420 keV can be attributed to the K-shell photoelectrons from the lead target produced by 511-keV rays of the two-quantum annihilation process. A shoulder in the vicinity of 500 keV may be due to the contributions from the L-shell photoelectrons by this process and partially from a sum effect of the K-shell photoelectrons and K x rays from lead. The second shoulder in the vicinity of 600 keV may be explained as due to pulses caused by the direct interaction of 511-keV radiation with the silicon detector and by a sum effect of this radiation and K x rays from lead. The observed spectrum in the higher energy region may be understood as the effects of γ rays resulting from the two-quantum annihilation in flight in lead. In order to evaluate the background contributions from the strayed γ rays and the natural background, a series of measurements were performed under a similar experimental arrangement, but with a Na^{22} source covered by a Lucite plate of 8 mm thickness so as to stop positrons. The background thus observed is shown by open circles in Fig. 5.

With an aim to finding a peak due to the radiationless annihilation in lead in the vicinity of an expected kinetic energy (1146 keV) of the K-shell electron ejected by this process for the K-K pair, 12-h measurements were carefully repeated many times in order to get good counting statistics within our scope. The total time of observation was about 400 h. In Fig. 6 is shown the electron spectrum in this energy region obtained after subtracting the strayed γ-ray and natural backgrounds. As shown in the figure, a small but evident peak is found in the region corresponding to the energies of the ejected electrons. An arrow, noted by 1146 keV, shows the position of a channel number corresponding to that for the peak observed when electrons of this energy are focused on the lead target. Hence, the kinetic energy of these electrons before entering the detector is about 1.02 MeV, owing to energy loss in the lead target foil.

In this energy region of the observed spectrum, in addition to a contribution from the annihilation process to be studied, there would exist three other possible sources of contributions, as follows: (1) internal-conversion electrons from a Na^{22} source; (2) photoelectrons and/or Compton recoil electrons ejected from the lead target by the photons from the two-quantum annihilation in flight in lead; (3) a similar contribution from the single-quantum annihilation in lead. Since the con-

version coefficient of the 1277-keV transition in Ne^{22} is very small, $(6.77\pm0.45)\times10^{-6}$,[11] and the electron-to-positron rejection ratio of our spectrometer is also very high (as mentioned in Sec. III), the possible contribution from the first cause can be neglected.

The maximum energy of photons created by the two-quantum annihilation in flight for 300-keV incident positrons is about 980 keV,[12] hence the maximum energy of the K-shell photoelectrons becomes about 900 keV. A few electrons out of those produced by L-shell photoelectric or Compton effect may have higher energy than 900 keV. Reflecting on these facts and the expected spectra discussed in the preceding section, the lower end of the peak in Fig. 6 is chosen to be at the channel corresponding to 900-keV electrons detected. Moreover, the experimental and background curves in the figure in the energy range between 900 and 980 keV are drawn so as to minimize contributions from these electrons.

As a predominant source of the background in the vicinity of the observed peak, the photoelectrons and Compton recoil electrons from the target produced by γ rays from the single-quantum annihilation should be estimated. The energy of the photon from this process is given by

$$E_\gamma = E_+ + E_B, \tag{25}$$

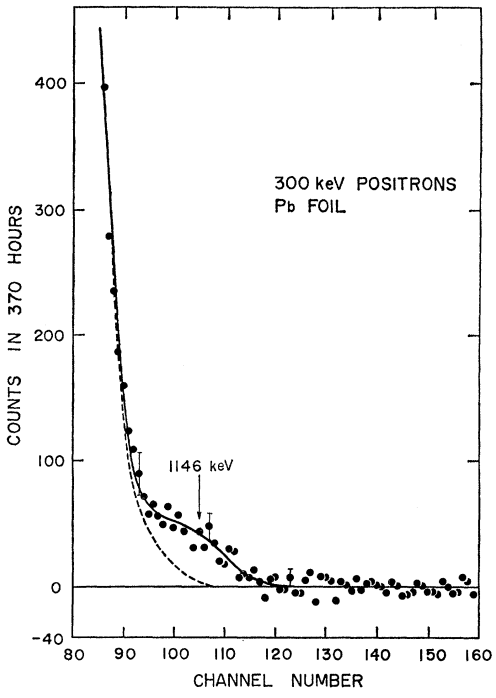

FIG. 6. Observed peak of the shell electrons ejected from a thin lead foil by the radiationless annihilation of 300-keV positrons. A K-shell electron ejected by this process with another K-shell electron in a lead atom is expected to have a kinetic energy of 1146 keV.

where E_+ is the total energy of an incident positron and E_B is the total energy of the shell electron involved. A contribution from the electrons ejected by the photons was estimated using the calculated cross section for the single-quantum annihilation reported by Johnson *et al.*[13] under an assumption that all the photons are created by this process at the source-side surface of the lead target. A contribution from such a process was found to be only about 10% of the observed counts at the channel number denoted by an arrow in Fig. 6 as the maximum evaluation. The background curve shown by a dashed curve in this figure is drawn by taking into account this estimation as well as the characteristics of the detector.

The experimental curve shown in Fig. 6 is drawn smoothly by combining the above facts and experimental points obtained as well as the expected electron spectrum evaluated in the preceding section. The profile of the observed net peak thus obtained has no shoulder and is somewhat different from the expected one. Owing to the poor statistics of our measurement no shoulder can be distinguished. However, the observed peak shown in Fig. 6 is interpreted as being due to the ejected shell electrons, including those from K, L, and M shells, by the radiationless annihilation of 300-keV positrons in lead.

Making use of the experimental data obtained by the present measurement, we have attempted to estimate the cross section for this annihilation process in lead. The cross section can be given by the following expression:

$$\sigma = \frac{(N_e/\epsilon_e)C_e}{n_F G P C_p (N_p/\epsilon_p)}. \tag{26}$$

The symbols in the expression are as follows:

N_e = the number of observed ejected shell electrons per unit time;
N_p = the number of 300-keV positrons incident on the lead target per unit time;
n_F = the effective number of lead atoms in the target per unit area;
G = the geometrical efficiency of the silicon detector for incident electrons from the lead target;
P = the peak-to-total ratio for incident electrons with the expected energy;
ϵ_p = the detection efficiency of the silicon detector for incident 300-keV positrons;
ϵ_e = the same for ejected shell electrons;
C_p = the correction factor for the effect of the finite target thickness for incident positrons; and
C_e = the same for ejected shell electrons.

N_e was obtained by measuring the area of the peak shown in Fig. 6. n_F is easily determined for the lead

[11] Y. Nakayama and H. Hirata, Nucl. Phys. **40**, 396 (1963).
[12] H. A. Bethe, Proc. Roy. Soc. (London) **A150**, 129 (1935).
[13] W. R. Johnson, D. J. Buss, and C. O. Carroll, Phys. Rev. **135**, A1232 (1964).

foil of 75.3 mg/cm² thickness. N_p, P, and ϵ_p/ϵ_e were estimated by the procedures described in Sec. III.

The geometrical efficiency G refers to the fraction of shell electrons emitted from the target foil that is detected by the solid detector. G must be calculated by taking account of the present geometry of the circular lead target foil (effective diameter is 6 mm) and the circular silicon detector of 8 mm diam as well as the angular distribution of the ejected shell electrons. Because this angular distribution $P(\theta)$ is very complicated, as shown in Sec. IV, the analytical calculation of G is extremely difficult. Therefore, we applied the Monte Carlo technique, which used random numbers to give the point of origin of annihilation and direction cosines using $P(\theta)$. The computer program ascertains whether or not a line with the randomly selected direction, originating at the randomly chosen point on a disk of the target foil, intersects a disk representing the detector. The calculated value of G thus obtained is 0.538±0.005.

As to evaluation of a correction factor C_e/C_p for the effect of the target thickness in Eq. (26), we had also to pursue a rather complicated procedure. This correction factor C_e/C_p can be defined as a ratio of the number of detected electrons estimated from Eq. (24) to that estimated from Eq. (19). Using Eqs. (19) and (24), the analytical expression of C_e/C_p can be obtained as

$$\frac{C_e}{C_p}=\frac{N_0T\sec\alpha\sum_{\text{all electron pairs}}\sigma(E_0)\int_{E\min}^{E\max}\int_{\alpha-\delta}^{\alpha+\delta}K(E_0,E'';T,\theta)P(\theta)\sin\theta\,d\theta dE''}{\sum_{\text{all electron pairs}}\int_{E\min}^{E\max}\int_0^T\int_0^{E_0}\int_{\alpha-\delta}^{\alpha+\delta}N(E,x)\sigma(E)K(E,E'';x,\theta)P(\theta)\sin\theta\,d\theta dEdxdE''}. \tag{27}$$

In the present work, since the lower limit of the observed peak portion is chosen at 900 keV for the reason mentioned before, this energy should be taken as $E_{\min}$. For $E_{\max}$ we can adopt a value for the higher-energy end of the expected spectrum given by Eq. (24), i.e., 1400 keV, shown by the dashed curve in Fig. 4. The value of C_e/C_p can be estimated by measuring a ratio of areas under the curves of electron spectra shown in Fig. 4, but limited within an energy range from 900 to 1400 keV. Moreover, it is noted that the integration of E'' in the numerator in Eq. (27) must be carried out only for the peak portion of the electron spectrum in this energy region. The lower-energy side of the peak (dashed curve) is presumed as shown by the dotted curve in Fig. 4. This peak is considered to be the total absorption peak due to the ejected shell electrons in the case where no effect of the target thickness is taken into account. The numerical value of C_e/C_p thus estimated and used in the present work is 1.4±0.1. The error given is evaluated only from the counting statistics involved.

By inserting numerical values of the factors concerned into the right-hand side of Eq. (26), we have obtained the total cross section for the radiationless annihilation of 300-keV positrons in lead as

$$\sigma_{\text{exptl}}=0.8_{-0.3}^{+0.4}\times10^{-26}\text{ cm}^2,$$

as a sum of those for K-K, K-L, K-M, and L-L pairs of shell electrons. The error shown is mainly ascribed to an uncertainty in the determination of N_e, caused by the poor statistics of our measurements. For the numerical value of the denominator of Eq. (27) for C_e/C_p, we adopted the area under the solid curve between 900 and 1400 keV in Fig. 4. However, examining our observed spectrum of the ejected electrons shown in Fig. 6, a value somewhat smaller than that which we adopted may be more reasonable for the present purpose. This means that a slightly larger value of C_e/C_p may give a closer approximation for this correction factor. The asymmetry of the error, larger "plus" error, in our experimental cross section reflects this fact. This value of the total cross section is about one-third of our preliminary result[3] reported in 1965. This is caused by more careful reexamining of the experimental data as well as by introducing improved evaluations of the geometrical efficiency of the detector, G. In addition a correction factor C_e/C_p has been used.

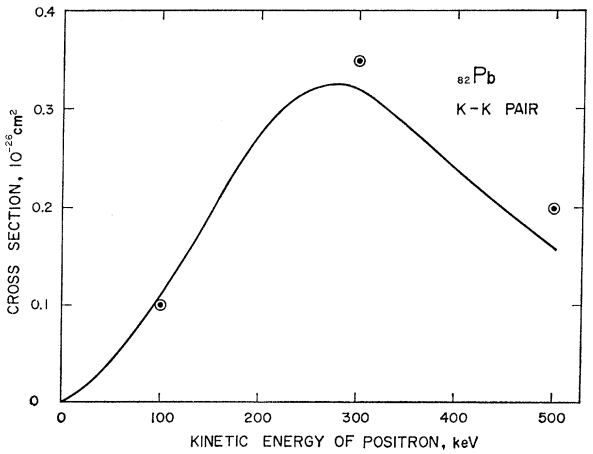

FIG. 7. Calculated cross section for the radiationless annihilation of positrons by the K-K pair of shell electrons in a lead atom as a function of kinetic energy of positron. Circles are the values calculated by Massey and Burhop (Ref. 2).

This has been estimated by necessary measurements of the positron and electron energy distribution in lead foils based upon reasonable assumptions, as described above.

Calculations to obtain the theoretical value of the cross section for this process in lead were carried out using the method described in Sec. II. Equation (2) was programmed for our computer[10] for $_{82}$Pb, for an incident positron energy $E_+=1.587$ (kinetic energy= 300 keV), and for the K, L, and M shells. Another program was also written for $_{82}$Pb and the K shell, but for various incident positron energies. In both cases the sums over κ_1, κ_2, and l were terminated at $|\kappa_1|=3$, $|\kappa_2|=5$, and $l=5$. All other parameters were determined in terms of $|\kappa_1|$ through the selection rules contained in the angular momentum coupling coefficients.

In Fig. 7 is shown the calculated cross section for the K-K pair of the shell electrons in a lead atom as a function of the kinetic energy of the incident positron. Our results agree well with earlier results given by Massey and Burhop,[2] which are represented by circles in the figure.

In Table I are given the calculated cross sections for different pairs of the shell electrons in a lead atom for a positron having an incident energy of 300 keV. We have not calculated the values for K-M_{II}, L_I-M_I, L_{II}-L_{II}, and other pairs of the shell electrons, as these are supposed to be considerably smaller as compared with those given in Table I. In the last column is also given our experimental result for comparison.

Both experimental and calculated results obtained by the present work agree with each other within the experimental error. The error inherent in the experimental result is rather large, and our calculations are based in part on some untested assumptions; nevertheless, the present work has provided the experimental evidence of this mode of positron annihilation and assisted comprehension of the process.

It should be noted here that we have also attempted to observe this phenomenon by 300-keV incident positrons using a thin tantalum foil of 89.5 mg/cm^2, but found no appreciable evidence. This fact may suggest that Z dependence of the cross section would be larger than Z^2.

Reflecting on the present work, it is hoped that a further experimental study be made, using more elaborate methods, a stronger positron beam, and thinner targets, to provide additional information on this process. Experimental and theoretical studies on the angular distribution of the ejected shell electrons and the Z dependence of the process would also be of great interest.

TABLE I. Calculated values of cross sections for the radiationless annihilation of 300-keV positrons for K-K, K-L, K-M, and L-L pairs of shell electrons in lead, and comparison with an experimental total cross section.

Shell electron pair	Kinetic energy of ejected shell electrons[a] (keV)	σ_{calc} (10^{-26} cm^2)	σ_{exptl} (10^{-26} cm^2)
K-K	1146.0	0.322	
K-L_I	1218.1	0.117	
K-L_{II}	1218.8	0.085	
K-L_{III}	1221.0	0.080	
K-M_I	1230.1	0.028	
L_I-L_I	1290.2	0.016	
L_I-L_{II}	1290.9	0.037	
L_I-L_{III}	1293.1	0.042	
		total 0.727	$0.8_{-0.3}^{+0.4}$

[a] Calculated by Eq. (1) using binding energies of K-, L_I-, L_{II}-, L_{III}-, and M_I-shell electrons in lead being 88.0, 15.9, 15.2, 13.0, and 3.9 keV, respectively [*Nuclear Spectroscopy Tables*, edited by A. H. Wapstra, G. J. Nijgh, and R. van Lieshout (North-Holland Publishing Co., Amsterdam, 1959)].

ACKNOWLEDGMENTS

The authors are indebted to Dr. J. C. Charlton of the Radiochemical Centre, Amersham, England for his cooperation in preparing a Na^{22} solution of high specific activity used in the present work. Thanks are also due to Dr. W. R. Johnson of University of Notre Dame for communicating to us prior to publication his theoretical work on the angular distribution of single-quantum annihilation radiation.

APPENDIX

From Eq. (2) the cross section σ can be written in the following form:

$$\sigma=8\pi e^4E_+E_-(p_-/p_+)\sum_{\kappa_1\kappa_2 l}\{k_0^2B\bar{B}-k_0k_0'(B\bar{C}+\bar{B}C)+k_0'^2C\bar{C}\}(1-\tfrac{1}{2}\delta_{k_0,k_0'}), \tag{A1}$$

where k_0' is the energy transfer in the transition corresponding to the matrix element C and $B\bar{B}$ is

$$B\bar{B}=\sum_{i=1}^{4}\sum_{j=1}^{4}B_i\bar{B}_jI_{\kappa_1\kappa_2 l}{}^{(i)}I_{\kappa_1\kappa_2\bar{l}}{}^{(j)*}+\sum_{i=1}^{4}\sum_{j=5}^{8}[(\pm)B_i\bar{B}_j'I_{\kappa_1\kappa_2 l}{}^{(i)}I_{\kappa_1\kappa_2\bar{l}}{}^{(j)*}+(\pm)B_j'\bar{B}_iI_{\kappa_1\kappa_2 l}{}^{(j)}I_{\kappa_1\kappa_2\bar{l}}{}^{(i)*}]$$
$$+\sum_{i=5}^{8}\sum_{j=5}^{8}(\pm)B_i'\bar{B}_j'I_{\kappa_1\kappa_2 l}{}^{(i)}I_{\kappa_1\kappa_2\bar{l}}{}^{(j)*}. \tag{A2}$$

In this expression $(\pm)$ denotes a sign depending on i and j. B_i is $(4\pi)^{3/2}$ times $P_{\kappa_1 m_1}{}^*(\hat{p}_+,-\hat{\xi}_1)P_{\kappa_2 m_2}{}^*(\hat{p}_-,-\hat{\xi}_2)B_{\kappa_1\kappa_2\kappa_3\kappa_4}$

given in Eq. (12). B_i and $\bar{B}_i$ are related by the substitutions

$$l \leftrightarrow \bar{l}, \qquad l_3 \leftrightarrow \bar{l}_3, \qquad l_4 \leftrightarrow \bar{l}_4.$$

$B\bar{C}$, $\bar{B}C$, and $C\bar{C}$ can be given by the expressions similar to Eq. (A2).

In Eq. (A2) products of coefficients of $I_{\kappa_1\kappa_2 l}^{(i)}$'s after summations over magnetic quantum numbers are given by

$$B_i\bar{B}_j = \frac{[j_1][j_2][j_3][j_4][l_1][l_2]}{[l]}([l_3][l_4][\bar{l}_3][\bar{l}_4])^{1/2}C(l_1l_3l;\,oo) \times C(l_2l_4l;\,oo)C(l_1\bar{l}_3l;\,oo)C(l_2\bar{l}_4l;\,oo)W(j_1j_3l_1l_3;\,l\tfrac{1}{2}) \times W(j_2j_4l_2l_4;\,l\tfrac{1}{2})W(j_1j_3l\bar{l}_3;\,l\tfrac{1}{2})W(j_2j_4l_2\bar{l}_4;\,l\tfrac{1}{2})\delta_{l,\bar{l}}, \quad \text{(A3)}$$

$$B_i\bar{B}_j' = (-1)^{j_3+j_4+l+\bar{l}}6[j_1][j_2][j_3][j_4][\bar{l}]([l_1][l_2][l_3][l_4][\bar{l}_3][\bar{l}_4])^{1/2}C(l_1l_3l;\,oo)C(l_2l_4l;\,oo)C(\bar{l}_3\bar{l}_1;\,oo)C(\bar{l}_4\bar{l}_2;\,oo) \times W(j_1j_3l_1l_3;\,l\tfrac{1}{2})W(j_2j_4l_2l_4;\,l\tfrac{1}{2})X\begin{pmatrix} \bar{l} & 1 & l \\ \bar{l}_3 & \frac{1}{2} & j_3 \\ l_1 & \frac{1}{2} & j_1 \end{pmatrix}X\begin{pmatrix} \bar{l} & 1 & l \\ \bar{l}_4 & \frac{1}{2} & j_4 \\ l_2 & \frac{1}{2} & j_2 \end{pmatrix}, \quad \text{(A4)}$$

$$B_i'\bar{B}_j' = (-1)^{l+\bar{l}}36[j_1][j_2][j_3][j_4][l][\bar{l}]([l_3][l_4][\bar{l}_3][\bar{l}_4])C(l_3ll_1;\,oo)C(l_4ll_2;\,oo)C(\bar{l}_3\bar{l}_1;\,oo)C(\bar{l}_4\bar{l}_2;\,oo) \times \sum_L [L]X\begin{pmatrix} l & 1 & L \\ l_3 & \frac{1}{2} & j_3 \\ l_1 & \frac{1}{2} & j_1 \end{pmatrix}X\begin{pmatrix} l & 1 & L \\ l_4 & \frac{1}{2} & j_4 \\ l_2 & \frac{1}{2} & j_2 \end{pmatrix}X\begin{pmatrix} \bar{l} & 1 & L \\ \bar{l}_3 & \frac{1}{2} & j_3 \\ l_1 & \frac{1}{2} & j_1 \end{pmatrix}X\begin{pmatrix} \bar{l} & 1 & L \\ \bar{l}_4 & \frac{1}{2} & j_4 \\ l_2 & \frac{1}{2} & j_2 \end{pmatrix}, \quad \text{(A5)}$$

where $X(abc;\,def;\,ghi)$ is the 9-j symbol and $B_i'\bar{B}_j'$ is the same form as $B_i\bar{B}_j'$.

The angular coupling coefficients in $B\bar{C}$ are expressed as

$$B_i\bar{C}_j = (-1)^{j_1+j_2+j_3+j_4+l+\bar{l}+1}[j_1][j_2][j_3][j_4][l_1][l_2]([l_3][l_4][\bar{l}_3][\bar{l}_4])^{1/2} \times C(l_1l_3l;\,oo)C(l_2l_4l;\,oo)C(l_1\bar{l}_4\bar{l};\,oo)C(l_2\bar{l}_3\bar{l};\,oo)W(j_1j_3l_1l_3;\,l\tfrac{1}{2})W(j_2j_4l_2l_4;\,l\tfrac{1}{2})W(j_1j_4l_1\bar{l}_4;\,\bar{l}\tfrac{1}{2}) \times W(j_2j_3l_2\bar{l}_3;\,\bar{l}\tfrac{1}{2})W(j_1j_3j_4j_2;\,l\bar{l}), \quad \text{(A6)}$$

$$B_i\bar{C}_j' = (-1)^{j_1+j_2+l+\bar{l}+1}6[j_1][j_2][j_3][j_4][\bar{l}]([l_1][l_2][l_3][l_4][\bar{l}_3][\bar{l}_4])^{1/2} \times C(l_1l_3l;\,oo)C(l_2l_4l;\,oo)C(\bar{l}_4\bar{l}_1;\,oo)C(\bar{l}_3\bar{l}_2;\,oo)W(j_1j_3l_1l_3;\,l\tfrac{1}{2})W(j_2j_4l_2l_4;\,l\tfrac{1}{2}) \sum_L [L]X\begin{pmatrix} \bar{l} & 1 & L \\ \bar{l}_4 & \frac{1}{2} & j_4 \\ l_1 & \frac{1}{2} & j_1 \end{pmatrix} \times X\begin{pmatrix} \bar{l} & 1 & L \\ \bar{l}_3 & \frac{1}{2} & j_3 \\ l_2 & \frac{1}{2} & j_2 \end{pmatrix}W(j_1j_3j_4j_2;\,lL), \quad \text{(A7)}$$

$$B_i'\bar{C}_j' = (-1)^{j_1+j_2+j_3+j_4+l+\bar{l}+1}36[j_1][j_2][j_3][j_4][l][\bar{l}]([l_3][l_4][\bar{l}_3][\bar{l}_4])^{1/2} \times C(l_3ll_1;\,oo)C(l_4ll_2;\,oo)C(\bar{l}_4\bar{l}_1;\,oo)C(\bar{l}_3\bar{l}_1;\,oo) \times \sum_{LL'}[L][L']X\begin{pmatrix} l & 1 & L \\ l_3 & \frac{1}{2} & j_3 \\ l_1 & \frac{1}{2} & j_1 \end{pmatrix}X\begin{pmatrix} l & 1 & L \\ l_4 & \frac{1}{2} & j_4 \\ l_2 & \frac{1}{2} & j_2 \end{pmatrix}X\begin{pmatrix} \bar{l} & 1 & L' \\ \bar{l}_4 & \frac{1}{2} & j_4 \\ l_1 & \frac{1}{2} & j_1 \end{pmatrix}X\begin{pmatrix} \bar{l} & 1 & L' \\ \bar{l}_3 & \frac{1}{2} & j_3 \\ l_2 & \frac{1}{2} & j_2 \end{pmatrix}W(j_1j_3j_4j_2;\,LL'). \quad \text{(A8)}$$

The coefficients for $\bar{B}C$ have the same forms as expressed by Eqs. (A6)–(A8).